Ultrasound neuromodulation of an anti-inflammatory pathway at the spleen produces sustained improvement of experimental pulmonary hypertension

Stefanos Zafeiropoulos MD MS*[1,2], Umair Ahmed MD*[2], Ibrahim T Mughrabi MD PhD[2], Naveen Jayaprakash PhD[2], Chrystal Chadwick BS[3], Anna Daytz BS[2], Alexandra Bekiaridou MD[2], Nafiseh Saleknezhad MD[2], Yemil Atish-Fregoso MD PhD[4], Kaitlin Carroll PhD[4], George Giannakoulas MD PhD[15], Yousef Al-Abed PhD[1,2], Christopher Puleo PhD[3], Mark Nicolls MD[6], Betty Diamond MD PhD[4,7], Stavros Zanos MD PhD[1,2,7]
(*) These two authors contributed equally to this study.

Authors' affiliation(s):
1. Elmezzi Graduate School of Molecular Medicine, Northwell Health, Manhasset, NY
2. Institute of Bioelectronic Medicine, Feinstein Institutes for Medical Research, Manhasset, NY
3. General Electric Global Research, Niskayuna, NY
4. Institute of Molecular Medicine, Feinstein Institutes for Medical Research, Manhasset, NY
5. Department of Cardiology, AHEPA University Hospital, Aristotle University School of Medicine, Thessaloniki, Greece
6. Division of Pulmonary, Allergy and Critical Care Medicine, Department of Medicine, Stanford University, Stanford, CA
7. Zucker School of Medicine at Hofstra/Northwell, Hempstead, NY

Corresponding author:
Stavros Zanos, MD, PhD
350 Community Drive, Manhasset, NY, 11030
E-mail: szanos@northwell.edu

Short title: Splenic ultrasound improves experimental pulmonary hypertension

Word count: 7549

Abstract

Rationale: Chronic inflammation is pathogenically implicated in pulmonary arterial hypertension (PAH), however, it has not been adequately targeted therapeutically.

Objectives: We investigated whether neuromodulation of an anti-inflammatory neuroimmune pathway using noninvasive, focused ultrasound stimulation of the spleen (sFUS) can improve experimental pulmonary hypertension (PH).

Methods: PH was induced in rats by SU5416 (20 mg/kg SQ) injection, followed by 21 (or 35) days of hypoxia (10% FiO_2). Animals were randomized to receive either daily, 12-min-long sessions of sFUS or sham-stimulation, for 14 days. Invasive hemodynamics, echocardiography, autonomic function parameters, lung and heart histology/immunohistochemistry, and lung single-cell-RNA sequencing were performed after treatment to assess effects of sFUS.

Results: Compared to sham, sFUS treatment reduces right ventricular (RV) systolic pressure by 25-30%; it improves RV function and indices of autonomic function. sFUS treatment reduces wall thickness in small pulmonary arterioles, suppresses inflammatory cell infiltration in lungs and RV fibrosis and hypertrophy, and lowers serum levels of brain natriuretic peptide. Beneficial effects persist for weeks after sFUS treatment discontinuation and are more robust when treatment is initiated earlier and delivered for longer. Selective ablation of the splenic nerve abolishes the therapeutic benefits of sFUS. sFUS treatment downregulates several inflammatory genes and pathways in nonclassical and classical monocytes, and macrophages in the lung; differentially expressed genes in those cell types are significantly enriched for genes associated with human PAH.

Conclusions: Noninvasive, sFUS treatment causes sustained improvement of hemodynamic, autonomic, laboratory and pathological manifestations of experimental PH, and downregulates inflammatory genes and pathways in the lung, many of which are relevant in human disease.

Keywords: inflammatory reflex; focused ultrasound; autonomic neuromodulation; Sugen-hypoxia model

Introduction

Pulmonary arterial hypertension (PAH) is a relatively rare but fatal disease, characterized by abnormal contraction and proliferation of smooth muscle cells in pulmonary arterioles, which along with neointimal formation, lead to a progressive increase in pulmonary vascular resistance and development of right heart failure. Current PAH-specific treatments act primarily by promoting pulmonary vasodilation and, despite improving symptoms and functional capacity, they neither alter the natural progression of the disease nor reduce mortality, which remains high (1, 2). Therefore, there is an urgent need for new and disease-modifying treatments. Chronic immune dysfunction and lung inflammation, which implicate cytokines, macrophages and lymphocytes, play a critical role in PAH pathogenesis by creating a microenvironment of exuberant cell growth and promoting intimal and medial hypertrophy (3-5). However, treatments targeting inflammation, including ligand traps and biologics, have only recently started being tested clinically (6-10). Thus, it remains unclear whether targeting inflammation could be an effective, possibly disease-modifying, therapeutic strategy in the treatment of PAH.

Inflammatory processes are regulated by local and systemic immune, hormonal and neural mechanisms, including autonomic neuroimmune pathways, which directly regulate immune cells through local release of neurotransmitters (11, 12). A well-studied neuroimmune pathway starts with vagal and sympathetic nerve fibers synapsing at abdominal ganglia and efferent, noradrenergic nerve fibers innervating the spleen (12). Upon activation of the pathway, norepinephrine is released from the splenic nerve in the spleen, causing splenic T-cells to secrete acetylcholine, which acts on alpha-7 cholinergic receptors on splenic macrophages and suppresses release of pro-inflammatory cytokines (12). Modulation of this pathway with electrical vagus nerve stimulation (VNS) reduces inflammation in several disease models (13), and, recently, in patients with rheumatoid arthritis (14). Electrical VNS was recently tested in a rat model of pulmonary hypertension (PH), improving pulmonary hemodynamics and suppressing cytokines and pathological markers of inflammation (15). However, the clinical significance of this approach may be limited due to off-target effects and the upfront risk of surgical implantation of a medical device (16, 17). Recently, an alternative approach for activating the neuroimmune pathway to suppress inflammation has emerged: low intensity focused ultrasound stimulation of the spleen (sFUS) (18, 19). sFUS is a non-invasive, organ-specific neuromodulation approach that activates the noradrenergic nerve terminals in the spleen and suppresses acute (19) and chronic systemic inflammation (20), to a similar extent as electrical VNS (19). This non-invasive approach may thus represent an anti-inflammatory

treatment, adjunct to PAH-specific treatments, in the hemodynamically sensitive population of PAH patients.

Methods

A detailed description of the materials and methods is provided in the Supplementary material.

Animal model of pulmonary hypertension (PH) and treatment cohorts

PH was induced in 62 male Sprague-Dawley rats (5-7 weeks, 150-200g, Charles River) using the Sugen-Hypoxia-Normoxia (SuHxNx) model, as previously described (21). The rats were randomly assigned to either receive sFUS or sham treatment in different cohorts. All procedures were approved by Institutional Animal Care and Use Committee of the Feinstein Institutes for Medical Research. The sFUS system is a custom-made machine consisting of transducer, a matching network, an RF power amplifier and a function generator.

PH endpoints assessment

Briefly, invasive right and left heart catheterizations, echocardiography, daily electrocardiogram recordings, lung and heart immunohistopathology, cytokines and brain natriuretic peptide measurements were performed.

Splenic nerve denervation

In a subset of animals ("splenic denervation cohort", n=8), we performed splenic nerve denervation (SND) on day 21 using surgical transection, local application of 100% ethanol and delivery of direct current.

Single-cell RNA sequencing (sc-RNA seq)

Sc-RNA seq analysis was performed using the Seurat R package (R Foundation for Statistical Computing). Known and canonical cell-type marker genes were used for the identification of cell types (23). Differentially expressed genes (DEGs) between treatment arms were determined for each cell type. Then, we performed gene-set enrichment analysis using hallmark pathways from the Molecular Signature Database to annotate DEGs for biological pathways as well as using human PAH-associated genes obtained from DisGeNET (24) and the Comparative Toxicogenomics Database (25) to establish human relevance.

Statistical analysis

All data are expressed as mean ± standard error of the mean (SE). Comparisons between two groups were made using t-test, one-way or two-way analysis of variance followed by

Bonferroni's post hoc test. A p-value <0.05 (after correction) was considered significant. All statistical analyses were performed with R Project for Statistical Computing (version 4.0.2).

Results

sFUS treatment improves pulmonary hemodynamics and reduces RV hypertrophy

Single or repeated sessions of sFUS suppress manifestations in animal models of acute or chronic inflammation, respectively (19, 20). We hypothesized that chronic sFUS treatment may suppress inflammatory aspects of PH pathogenesis and ameliorate manifestations of the disease in the SuHxNx rat model of PH. On day 1, animals injected with SU5416 subcutaneously and were then placed in a hypoxia chamber (FiO_2=10%) for 21 days, after which they were brought back into normoxia ("Hypoxia-Normoxia cohort", HxNx). To model a more severe disease phenotype, in another cohort, animals were kept inside the hypoxia chamber for 35 days ("Hypoxia-Hypoxia cohort", HxHx). In both cohorts, rats received daily sessions of sFUS or sham-stimulation from day 22 to day 35. The terminal experiment was performed on day 35 (Fig. 1A).

sFUS treatment significantly reduces right ventricular systolic pressure (RVSP), by approximately 30%, compared with sham-stimulation, in the HxNx cohort, and by about 20% in the HxHx cohort (Fig. 1B). Mean arterial pressure (Fig. 1C) and heart rate (Fig. 1D) are not affected by sFUS treatment, in either cohort. Even though RVSP was not measured longitudinally, the hemodynamic effect likely develops progressively over time: during insonification of the spleen, no acute effects on pulmonary or systemic hemodynamics are seen, in neither healthy nor hypertensive animals (Suppl. Fig. S1). In both HxNx and HxHx cohorts, sFUS treatment results in lower right atrial pressure (RAP) (Suppl. Fig. S2A) but does not change RV end-diastolic pressure (RVEDP) (Suppl. Fig. S2B).

Serum BNP levels are reduced in animals receiving sFUS treatment, in both HxNx and HxHx cohorts (Fig. 1E). In the HxNx cohort, after animals return to normoxia, they progressively gain weight which is significantly greater in animals receiving sFUS compared to sham (32.45% ± 1.89% vs 22.13% ± 0.95%; p = 0.002). Additionally, sFUS treatment results in reduced RV hypertrophy compared to sham treatment: Fulton index is significantly reduced in gross pathology (Fig. 1F), and RV free wall thickness is marginally non-significantly reduced in echocardiography (Fig. 1G). In these cohorts, sFUS treatment did not significantly improve

PAAT, PAAT/PAET and TAPSE (18.33 ±0.67 ms vs. 16.67 ±0.80, p=0.14; 0.21 ±0.01 vs 0.19 ± 0.01, p=0.28; and 2.56 mm ± 0.12 vs 2.37 ± 0.12, p=0.30, respectively, Suppl. Fig. S3).

sFUS treatment improves indices of autonomic function

PAH is associated with autonomic imbalance, consisting of increased sympathetic and decreased parasympathetic tone (22, 23). Commonly used markers of autonomic balance include heart rate variability (HRV) and baroreflex sensitivity (BRS) (24), both of which are reduced in the SuHxNx model (25) and in patients with PAH (26). Using daily ECG recordings and spectral analysis methods, we estimated the low-frequency (LF) and high-frequency (HF) components and calculated the LF/HF ratio, commonly used measures of HRV (Fig. 2A). sFUS-treated animals have significantly smaller LF/HF ratio at the end compared to the beginning of treatment; in contrast, LF/HF ratio does not change in sham-treated animals (Fig. 2B). Likewise, both LF and HF components improve in sFUS-treated animals but not in sham-treated animals (Suppl. Fig. S2C and S2D and Suppl. Table 1). At the end of treatment, sFUS-treated animals have lower LF/HF ratio compared to sham-treated animals (Fig. 2B). The reduction in LF/HF ratio in the sFUS-treated animals is first observed at day 31 and is sustained till the end of treatment (Fig. 2C). Across all animals in the two treatment arms and in both HxNx and HxHx cohorts, LF/HF ratio, measured at the end of treatment, is significantly correlated with RVSP (Fig. 2D and Suppl. Fig. S2E).

To determine BRS, phenylephrine (PE) was injected intravenously and the ratio of the resulting absolute value of change in heart rate (|ΔHR|) over the reflex change in systolic blood pressure (ΔSBP) was calculated (Suppl. Fig. S4): the higher the ratio, the more sensitive the reflex. sFUS treatment for 14 days is associated with higher BRS index (Fig 2E). Similar to the LF/HF ratio, BRS index is inversely correlated with RVSP (Fig. 2F), suggesting that HRV and BRS index could serve as markers of disease severity.

sFUS treatment improves vascular pathology and reduces inflammatory cell infiltration in the lung

In the SuHxNx model of PH, lungs exhibit pathological abnormalities, including increased wall thickness in pulmonary arterioles (PAs) (21, 27). To determine whether the hemodynamic benefits of sFUS treatment are accompanied by improvements in lung pathology, we performed morphometric analysis of PAs in H&E-stained lung samples (Fig. 3A). Compared to sham, animals treated with sFUS have reduced wall thickness in small PAs (Fig. 3B) but not in large PAs (Fig. 3C). Immunohistochemistry was used to quantify lung infiltration from inflammatory

cells, including monocytes and macrophages (CD68+) and T-cells (CD3+) (Fig. 3D and Suppl. Fig. S5). Counts of both cell types are significantly reduced in both the lung parenchyma (Fig. 3E) and perivascular areas (Fig. 3F) in sFUS-treated animals.

We measured levels of circulating inflammatory cytokines at the end of treatment. We found that sFUS-treated animals have reduced IFN-γ in serum; in contrast, tumor necrosis factor (TNF)-α and interleukin (IL)-6 in serum are similar to those in sham-treated animals (Suppl. Fig. S6). In spleen homogenates, pro-inflammatory cytokines levels are similar between sFUS- and sham-treated animals (Suppl. Fig. S6).

Therapeutic benefits of sFUS are sustained after discontinuation of treatment

To determine whether the therapeutic benefit of sFUS persists after discontinuation of treatment, in a separate HxNx cohort, right heart catheterization was performed on day 49, 14 days after the end of treatment ("extended follow-up" cohort; Fig. 4A). In this cohort, sFUS-treated animals maintain most of the hemodynamic benefit, since RVSP is still about 25% lower than in sham-treated animals (Fig. 4B); although RVSP values were higher in both groups compared with the cohort with the terminal experiment on day 35, reflecting the progression of disease in this model (28). RAP, LF/HF ratio, wall thickness of small PAs are reduced and RV function is improved in sFUS-treated compared to sham-treated animals (Fig. 4C-4F).

Earlier, longer treatment with sFUS results in more robust functional and structural therapeutic benefit

To determine whether time of initiation and duration of sFUS treatment impact the therapeutic benefit, in a separate HxNx cohort, sFUS (or sham) treatment was started on day 1 and was delivered daily for a total of 35 days, including the 21 days of hypoxia ("early treatment" cohort, Fig. 5A). In this cohort, sFUS robustly reduced RVSP, RAP and RVEDP (Fig. 5B, Suppl. Fig. S7A and S7B). Autonomic indices, BNP levels, wall thickness of PAs were also improved (Fig, 5C, 5D, Suppl. Fig. S7C and S7D) in sFUS-treated animals. Regarding the RV, sFUS improved free wall thickness, TAPSE, hypertrophy and fibrosis (Fig. 5E-5H and Suppl. Fig. S7E and S7F).

Selective ablation of the splenic nerve eliminates the therapeutic benefit of sFUS

sFUS acutely suppresses inflammation by increasing the release of norepinephrine from terminals of the splenic nerve (19) which is composed of noradrenergic post-ganglionic axons

(29). To determine whether the therapeutic effect of sFUS in PH is mediated by activation of the splenic nerve, we administered sFUS for 14 days in a cohort of HxNx animals which had received selective ablation of the splenic nerve, immediately before treatment initiation (day 21), (Fig. 6A and 6B and Suppl. Fig. S8). In this “splenic denervation cohort”, sFUS treatment does not reduce RVSP compared to sham stimulation (Fig. 6C). No differences in heart rate (Fig. 6D), LF/HF ratio (Fig. 6E) or wall thickness of small PAs (Fig. 6F) are observed between sFUS- and sham-treated animals.

sFUS treatment modulates transcription of inflammatory genes and pathways in immune cells in the lung

To screen for molecular mechanisms that could potentially mediate the therapeutic effects of sFUS in experimental PH, we performed scRNA-seq of lungs from 2 HxNx animals treated with sFUS and from 2 animals treated with sham stimulation. Sequencing of the 4 lungs profiled 7,870 cells after quality control steps, with even representation of groups. After clustering on the basis of transcriptomic similarity, 16 distinct cell types were identified, based on established markers for epithelial, stromal, lymphoid, and myeloid cell populations, and rare cell populations (Fig. 7A and Suppl. Fig. S9, S10). Lungs from the sFUS-treated animals have reduced proportion of T-cells and increased proportion of endothelial cells, compared with sham-treated animals (Fig. 7B). A total of 540 DEGs across 15 cell types were identified (false discovery rate <0.05) (Fig. 7C). We found that nonclassical monocytes (ncMono) and endothelial arterial 1 (EA1) cells have the most numerous DEGs (Fig. 7D) in the sFUS-treated animals. Pathway enrichment of DEGs revealed cell type–specific alterations of several inflammation-related pathways in different immune cell populations (Fig. 7E, Suppl. Fig. S11). Notably, the most cell-specific downregulated pathways include the TNFa/NF-kB signaling in interstitial (iMF) and alveolar macrophages (aMF), ncMono, classical monocytes (cMono), T-regulatory cells, CD4+ T-naïve cells and endothelial capillary cells and the inflammatory response in iMF and cMono (Fig. 7F, Suppl. Fig. S12). Conversely, IFN-alpha response in ncMono and neutrophils are the most upregulated cell-specific pathways (Fig. 7F, Suppl. Fig. S12). The same sc-RNAseq analysis was performed for 2 healthy vs. 2 hypertensive rats: the TNF via NF-Kb signaling pathway in ncMonos is the most upregulated in animals with PH (Suppl. Fig. S13), which is consistent with the published literature (30).

Integrative Analysis of rat scRNA-seq DEGs with human PAH-associated genes suggests possible clinical relevance of sFUS treatment

We performed an integrative analysis of rat scRNA-seq DEGs with human genes that are known to be associated with PAH. We identified genes implicated in human PAH from DisGeNET and the Comparative Toxicogenomics Database and tested rat DEGs for enrichment of these genes. We noticed significant enrichment of rat scRNA-seq DEGs in human PAH-associated genes from both databases, in myeloid cells, including iMF, cMono, ncMonos and aMF (Fig. 7G). We also noticed marked enrichment of human PAH-associated genes in the leading genes accounting for the downregulation of the TNFa via NF-kB pathway in the ncMonos (Fig. 7H).

Discussion

In this study of a noninvasive, ultrasound-based, anti-inflammatory treatment of experimental PH, we document robust and sustained improvement in many clinically relevant hemodynamic parameters (RVSP, RAP), autonomic indices (HRV and BRS) and biomarkers with prognostic value (BNP), indicating a translational potential for this bioelectronic therapy in human PAH. In addition, we show that sFUS suppresses inflammatory genes and pathways that are implicated in human PAH. To the best of our knowledge, this is the first report of preclinical efficacy of a noninvasive, ultrasound-based neuromodulation therapy in any cardiovascular or pulmonary disease, and more specifically in PH, with indications for translational relevance to human PAH.

Mechanisms of sFUS neuromodulation

Recent studies have demonstrated that sFUS reduces markers of inflammation in animal models of endotoxemia, pneumonia, inflammatory arthritis, colitis and acute renal ischemia-reperfusion injury, implicating activation of the anti-inflammatory neuroimmune pathway at the spleen (19, 20, 31, 32). Accordingly, we find that the therapeutic effect of sFUS on PH is eliminated by selective splenic denervation (Fig. 6), similarly to past studies of VNS in acute inflammation (33). The splenic nerve is comprised of noradrenergic, efferent axons of ganglionic neurons in the celiac plexus, which regulate the function of immune cell populations in the spleen (12). It is likely that sFUS depolarizes axonal terminals in the spleen to augment release of norepineprhine and activate the neuroimmune pathway—even though our study did not directly address this mechanism. Low intensity, focused ultrasound delivered to the brain produces mechanical waves that excite neurons via mechanosensitive ion channels, including

TRPP1/2, TRPC1, and Piezo1 (34). Similarly, FUS of the hepatoportal nerve plexus in animal models of diabetes restores glucose homeostasis via activation of TRPA1-positive, afferent nerve fibers (35). Notably, the abovementioned mechanosensitive ion channels are expressed in peripheral ganglia, in the vagus nerve and in some spinal nerves (36); the same channels are not expressed in other peripheral nerves, such as sciatic nerve, in which FUS does not elicit nerve responses (37).

Furthermore, we found no evidence of a direct hemodynamic effect of sFUS in the systemic or the pulmonary circulation (Suppl. Fig. S1), suggesting that the therapeutic effect of sFUS in PH is unlikely to be mediated by a direct effect on vascular tone or intravascular volume. Our finding that sFUS does not elicit acute hemodynamic effects has translational significance, as it suggests that this therapy may be safe in PAH patients, many of whom are easily compromised hemodynamically.

Immunological effects of sFUS in experimental PH

After an acute inflammatory challenge, a single session of sFUS suppresses the rise in TNF in the spleen and in whole blood of rodents (19). Similarly, 2 weeks of pretreatment with daily sFUS before an acute inflammatory challenge results in reduced, compared to sham treatment, transcript levels of *Tnf* and associated genes (18), suggesting that repeated sFUS may suppress gene expression across multiple molecular components of the innate immune response. Notably, our group has shown that sFUS also suppresses TNF release in response to ex-vivo inflammatory challenge from the peripheral blood mononuclear cells in healthy human subjects (unpublished data, Zanos et al). Together with our finding that sFUS suppresses transcription of several inflammatory pathways in myeloid cells in the lung (Fig. 7), this converging evidence suggests that neuroimmune activation with sFUS may modulate widespread immune pathways and cell types in the spleen, which in turn manifest as systemic and organ-specific anti-inflammatory effects.

In our study, we found pathologic and transcriptomic evidence for reduced inflammation in the lung. Macrophage perivascular infiltrates and increased expression of inflammatory genes play a critical role in pulmonary vasculature remodeling in PAH (3, 30). Regulation of lung inflammation by the autonomic nervous system has received relatively limited attention in PAH. Augmentation of parasympathetic activity with electrical VNS or pyridostigmine resulted in improved hemodynamics, autonomic balance and attenuated cardiac and pulmonary vascular remodeling in experimental PH (15, 25). In both those reports, the beneficial effects of augmentation of parasympathetic activity were attributed mainly to reduced inflammation (15,

25), even though the neuroimmune pathways for that effect remain unclear. In our report, sFUS engages a well-defined, efferent neural pathway at the spleen, with subsequent anti-inflammatory effects, directly implicating the autonomic control of inflammation in the pathogenesis and progression of experimental PH. Furthermore, serum levels of the proinflammatory cytokine IFN-γ, a key regulator of macrophage activation through the JAK/STAT signaling pathway (38), was reduced. We found no effect in the levels of pro-inflammatory cytokines in serum or in spleen (Suppl. Fig. S6), which could potentially be attributed to the overall low circulating levels of these cytokines in our model of PH or an effect of sFUS on cell trafficking rather than on soluble mediators of inflammation.

Therapeutic effects of sFUS may have relevance for human PAH

We evaluated therapeutic effects of sFUS in a well-established animal model of PAH, using several clinically-relevant endpoints. The SuHxNx model in rats shares several common features with PAH in humans, including pulmonary hemodynamics (27, 28), pathological findings in the lung and heart (21), and abnormalities in gene expression (9, 30). In addition, efficacy of therapies tested with this model has been frequently associated with responsiveness in humans with PAH (9, 39). In our study, sFUS reduces RVSP by ~20-30% in animal cohorts with different severity of PH (Fig. 1), RAP, which is the strongest predictor of survival in PAH (40), and serum BNP levels, a biomarker used in risk stratification of PAH (41).

sFUS improves lung vascular pathology; it also improves heart pathology, including fibrosis, but it is unclear if that is a direct effect of sFUS on the RV, or a secondary effect of reduced afterload. Treatment with sFUS improves indices of autonomic tone that are commonly impaired in PAH patients (42), similarly to other bioelectronic and pharmacologic therapies targeting the parasympathetic system (15, 25). Our observation that both HRV and BRS correlate with pulmonary hemodynamics (Fig. 2) suggests that such noninvasive autonomic markers may prove useful in the evaluation and risk stratification of PAH patients. Unlike standard vasodilator therapies, the therapeutic benefits of sFUS persist for at least 14 days after treatment cessation, suggesting a potential disease-modifying effect of sFUS. Only one other study has demonstrated sustained therapeutic benefit after treatment cessation in experimental PH and, interestingly, that therapy targets activin-driven inflammation in pulmonary vascular remodeling (9). Development of disease-modifying therapies in PAH has been a challenge and sFUS warrants further study toward that goal.

We identified the TNFa/NF-kB signaling pathway in myeloid cells to be strongly downregulated by sFUS (Fig. 7). scRNA sequencing studies in lungs in the SuHxNx model

show that the same pathway is most prominently upregulated, particularly in ncMonos (30). Additionally, TNF signaling via NFkB is a major pathway associated with PAH in humans and DEGs in ncMonos in the SuHxNx model are most highly enriched for human PAH-associated genes (30). Notably, in our study, DEGs in myeloid cells were significantly enriched for human PAH-associated genes; many of DEGs were also enriched in the leading genes of TNFa/NF-kB signaling pathway of ncMonos. We observed upregulation of the IFN-alpha response by sFUS (Fig. 7), a pathway downregulated in the monocrotaline model of experimental PH (30). Excess IFN signaling may contribute to PAH (43) and exogenous IFN-alpha improved experimental PH and decreased proliferation in human pulmonary arterial endothelial and smooth muscle cells in vitro (44). All these findings suggest that the anti-inflammatory and immunomodulatory effects of sFUS may have clinical significance in human PAH and warrant further investigations.

Limitations

Our study does not provide detailed mechanistic insights into the possible alterations in splenic immune cell function, and how such alterations impact the PH pathogenesis. Additionally, preclinical models might have limited predictive power for clinical outcomes.

Acknowledgments

The authors would like to thank Drs, Valentin Pavlov, Lance Becker, Theodoros Zanos, Kevin Tracey, Sangeeta Chavan, Anne Davidson, Annette Lee, Christine Metz, and Peter Gregersen, and Mr. Houman Khalili, Jose Mathew, for their critical appraisal of and comments on the manuscript.

Funding source

This study was partially funded through a grant from United Therapeutics Corp. to Stavros Zanos (“Bioelectronic treatment of pulmonary hypertension”).

Disclosures

The authors have nothing to disclose.

Impact

The hemodynamic, autonomic, pathologic and transcriptomic effects of sFUS in PH indicate a clinically significant and sustained benefit and highlight the critical role of inflammatory and immune responses in PH progression, suggesting new therapeutic targets beyond vasodilators. sFUS could improve a plethora of clinical endpoints and provide a disease-modifying effect in

patients with PAH. Therefore, our study explores a new anti-inflammatory approach to target a novel pathway of PAH pathogenesis, and sFUS could advance the field of PAH therapeutics and bioelectronic therapeutics in general.

Authors' contribution

SZaf, UA, ITM, MN, BD, YA, GG, CP, and Szan contributed to the conception or design of the work. SZaf, UA, ITM, NJ, CC, AD, AB, NS, YAF and KC contributed to the acquisition, analysis, or interpretation of data for the work. SZaf, UA and SZan drafted the manuscript. ITM, NJ, CC, AD, AB, NS, YAF, KC, GG, YA, CP, MK, and BD critically revised the manuscript. All gave final approval and agreed to be accountable for all aspects of work ensuring integrity and accuracy.

References

1. Hassoun PM. Pulmonary Arterial Hypertension. *New England Journal of Medicine* 2021; 385: 2361-2376.
2. Chang KY, Duval S, Badesch DB, Bull TM, Chakinala MM, De Marco T, Frantz RP, Hemnes A, Mathai SC, Rosenzweig EB, Ryan JJ, Thenappan T, Allen R, Bartolome S, Benza R, Cadaret L, Eggert M, Elwing J, Fineman J, Foley R, Ford HJ, Hirsch R, Grinnan J, Ivy DD, Kawut S, Kennedy J, Klinger J, Leary P, Mazimba S, Ramani G, Raina A, Runo J, Swisher J, Varghese N, White RJ, Williamson T, Yung D, Zamanian R, Zwicke D. Mortality in Pulmonary Arterial Hypertension in the Modern Era: Early Insights From the Pulmonary Hypertension Association Registry. *Journal of the American Heart Association* 2022; 11: e024969.
3. Rabinovitch M, Guignabert C, Humbert M, Nicolls MR. Inflammation and Immunity in the Pathogenesis of Pulmonary Arterial Hypertension. *Circulation Research* 2014; 115: 165-175.
4. Marsh LM, Jandl K, Grunig G, Foris V, Bashir M, Ghanim B, Klepetko W, Olschewski H, Olschewski A, Kwapiszewska G. The inflammatory cell landscape in the lungs of patients with idiopathic pulmonary arterial hypertension. *Eur Respir J* 2018; 51.
5. Nicolls MR, Voelkel NF. The Roles of Immunity in the Prevention and Evolution of Pulmonary Arterial Hypertension. *American Journal of Respiratory and Critical Care Medicine* 2016; 195: 1292-1299.
6. Humbert M, Guignabert C, Bonnet S, Dorfmüller P, Klinger JR, Nicolls MR, Olschewski Andrea J, Pullamsetti SS, Schermuly RT, Stenmark Kurt R, Rabinovitch M. Pathology and pathobiology of pulmonary hypertension: state of the art and research perspectives. *European Respiratory Journal* 2019; 53: 1801887.
7. Toshner M, Church C, Harbaum L, Rhodes C, Villar Moreschi SS, Liley J, Jones R, Arora A, Batai K, Desai AA, Coghlan JG, Gibbs JSR, Gor D, Gräf S, Harlow L, Hernandez-Sanchez J, Howard LS, Humbert M, Karnes J, Kiely DG, Kittles R, Knightbridge E, Lam B, Lutz KA, Nichols WC, Pauciulo MW, Pepke-Zaba J, Suntharalingam J, Soubrier F, Trembath RC, Schwantes-An TL, Wort SJ, Wilkins MR, Gaine S, Morrell NW, Corris PA. Mendelian randomisation and experimental medicine approaches to interleukin-6 as a drug target in pulmonary arterial hypertension. *Eur Respir J* 2022; 59.
8. Trankle CR, Canada JM, Kadariya D, Markley R, De Chazal HM, Pinson J, Fox A, Van Tassell BW, Abbate A, Grinnan D. IL-1 Blockade Reduces Inflammation in Pulmonary Arterial Hypertension and Right Ventricular Failure: A Single-Arm, Open-Label, Phase IB/II Pilot Study. *Am J Respir Crit Care Med* 2019; 199: 381-384.
9. Joshi SR, Liu J, Bloom T, Karaca Atabay E, Kuo T-H, Lee M, Belcheva E, Spaits M, Grenha R, Maguire MC, Frost JL, Wang K, Briscoe SD, Alexander MJ, Herrin BR, Castonguay R, Pearsall RS, Andre P, Yu PB, Kumar R, Li G. Sotatercept analog suppresses inflammation to reverse experimental pulmonary arterial hypertension. *Scientific Reports* 2022; 12: 7803.
10. Humbert M, McLaughlin V, Gibbs JSR, Gomberg-Maitland M, Hoeper MM, Preston IR, Souza R, Waxman A, Escribano Subias P, Feldman J, Meyer G, Montani D, Olsson KM, Manimaran S, Barnes J, Linde PG, de Oliveira Pena J, Badesch DB. Sotatercept for the Treatment of Pulmonary Arterial Hypertension. *New England Journal of Medicine* 2021; 384: 1204-1215.
11. Murray K, Rude KM, Sladek J, Reardon C. Divergence of neuroimmune circuits activated by afferent and efferent vagal nerve stimulation in the regulation of inflammation. *J Physiol* 2021.
12. Tracey KJ. The inflammatory reflex. *Nature* 2002; 420: 853-859.

13. Cheng J, Shen H, Chowdhury R, Abdi T, Selaru F, Chen JDZ. Potential of Electrical Neuromodulation for Inflammatory Bowel Disease. *Inflammatory Bowel Diseases* 2019; 26: 1119-1130.
14. Marsal S, Corominas H, de Agustín JJ, Pérez-García C, López-Lasanta M, Borrell H, Reina D, Sanmartí R, Narváez J, Franco-Jarava C, Peterfy C, Narváez JA, Sharma V, Alataris K, Genovese MC, Baker MC. Non-invasive vagus nerve stimulation for rheumatoid arthritis: a proof-of-concept study. *The Lancet Rheumatology* 2021; 3: e262-e269.
15. Yoshida K, Saku K, Kamada K, Abe K, Tanaka-Ishikawa M, Tohyama T, Nishikawa T, Kishi T, Sunagawa K, Tsutsui H. Electrical Vagal Nerve Stimulation Ameliorates Pulmonary Vascular Remodeling and Improves Survival in Rats With Severe Pulmonary Arterial Hypertension. *JACC Basic Transl Sci* 2018; 3: 657-671.
16. Ntiloudi D, Qanud K, Tomaio JN, Giannakoulas G, Al-Abed Y, Zanos S. Pulmonary arterial hypertension: the case for a bioelectronic treatment. *Bioelectron Med* 2019; 5: 20.
17. Ahmed U, Chang Y-C, Zafeiropoulos S, Nassrallah Z, Miller L, Zanos S. Strategies for precision vagus neuromodulation. *Bioelectronic Medicine* 2022; 8: 9.
18. Cotero V, Miwa H, Graf J, Ashe J, Loghin E, Di Carlo D, Puleo C. Peripheral Focused Ultrasound Neuromodulation (pFUS). *Journal of Neuroscience Methods* 2020; 341: 108721.
19. Cotero V, Fan Y, Tsaava T, Kressel AM, Hancu I, Fitzgerald P, Wallace K, Kaanumalle S, Graf J, Rigby W, Kao T-J, Roberts J, Bhushan C, Joel S, Coleman TR, Zanos S, Tracey KJ, Ashe J, Chavan SS, Puleo C. Noninvasive sub-organ ultrasound stimulation for targeted neuromodulation. *Nature Communications* 2019; 10: 952.
20. Zachs DP, Offutt SJ, Graham RS, Kim Y, Mueller J, Auger JL, Schuldt NJ, Kaiser CRW, Heiller AP, Dutta R, Guo H, Alford JK, Binstadt BA, Lim HH. Noninvasive ultrasound stimulation of the spleen to treat inflammatory arthritis. *Nature Communications* 2019; 10: 951.
21. Abe K, Toba M, Alzoubi A, Ito M, Fagan KA, Cool CD, Voelkel NF, McMurtry IF, Oka M. Formation of plexiform lesions in experimental severe pulmonary arterial hypertension. *Circulation* 2010; 121: 2747-2754.
22. Velez-Roa S, Ciarka A, Najem B, Vachiery J-L, Naeije R, Borne Pvd. Increased Sympathetic Nerve Activity in Pulmonary Artery Hypertension. *Circulation* 2004; 110: 1308-1312.
23. Ciarka A, Doan V, Velez-Roa S, Naeije R, Borne Pvd. Prognostic Significance of Sympathetic Nervous System Activation in Pulmonary Arterial Hypertension. *American Journal of Respiratory and Critical Care Medicine* 2010; 181: 1269-1275.
24. Zygmunt A, Stanczyk J. Methods of evaluation of autonomic nervous system function. *Arch Med Sci* 2010; 6: 11-18.
25. da Silva Gonçalves Bós D, Van Der Bruggen CEE, Kurakula K, Sun XQ, Casali KR, Casali AG, Rol N, Szulcek R, Dos Remedios C, Guignabert C, Tu L, Dorfmüller P, Humbert M, Wijnker PJM, Kuster DWD, van der Velden J, Goumans MJ, Bogaard HJ, Vonk-Noordegraaf A, de Man FS, Handoko ML. Contribution of Impaired Parasympathetic Activity to Right Ventricular Dysfunction and Pulmonary Vascular Remodeling in Pulmonary Arterial Hypertension. *Circulation* 2018; 137: 910-924.
26. Yi HT, Hsieh YC, Wu TJ, Huang JL, Lin WW, Liang KW, Su CS, Tsai WJ, Wang KY. Heart rate variability parameters and ventricular arrhythmia correlate with pulmonary arterial pressure in adult patients with idiopathic pulmonary arterial hypertension. *Heart Lung* 2014; 43: 534-540.
27. de Raaf MA, Schalij I, Gomez-Arroyo J, Rol N, Happé C, de Man FS, Vonk-Noordegraaf A, Westerhof N, Voelkel NF, Bogaard HJ. SuHx rat model: partly reversible pulmonary hypertension and progressive intima obstruction. *European Respiratory Journal* 2014; 44: 160.

28. Toba M, Alzoubi A, O'Neill KD, Gairhe S, Matsumoto Y, Oshima K, Abe K, Oka M, McMurtry IF. Temporal hemodynamic and histological progression in Sugen5416/hypoxia/normoxia-exposed pulmonary arterial hypertensive rats. *American Journal of Physiology-Heart and Circulatory Physiology* 2013; 306: H243-H250.
29. Verlinden TJM, van Dijk P, Hikspoors J, Herrler A, Lamers WH, Köhler SE. Innervation of the human spleen: A complete hilum-embedding approach. *Brain, Behavior, and Immunity* 2019; 77: 92-100.
30. Hong J, Arneson D, Umar S, Ruffenach G, Cunningham CM, Ahn IS, Diamante G, Bhetraratana M, Park JF, Said E, Huynh C, Le T, Medzikovic L, Humbert M, Soubrier F, Montani D, Girerd B, Trégouët DA, Channick R, Saggar R, Eghbali M, Yang X. Single-Cell Study of Two Rat Models of Pulmonary Arterial Hypertension Reveals Connections to Human Pathobiology and Drug Repositioning. *Am J Respir Crit Care Med* 2021; 203: 1006-1022.
31. Gigliotti JC, Huang L, Ye H, Bajwa A, Chattrabhuti K, Lee S, Klibanov AL, Kalantari K, Rosin DL, Okusa MD. Ultrasound prevents renal ischemia-reperfusion injury by stimulating the splenic cholinergic anti-inflammatory pathway. *J Am Soc Nephrol* 2013; 24: 1451-1460.
32. Ahmed U, Graf JF, Daytz A, Yaipen O, Mughrabi I, Jayaprakash N, Cotero V, Morton C, Deutschman CS, Zanos S, Puleo C. Ultrasound Neuromodulation of the Spleen Has Time-Dependent Anti-Inflammatory Effect in a Pneumonia Model. *Frontiers in Immunology* 2022; 13.
33. Rosas-Ballina M, Ochani M, Parrish WR, Ochani K, Harris YT, Huston JM, Chavan S, Tracey KJ. Splenic nerve is required for cholinergic antiinflammatory pathway control of TNF in endotoxemia. *Proceedings of the National Academy of Sciences* 2008; 105: 11008-11013.
34. Yoo S, Mittelstein DR, Hurt RC, Lacroix J, Shapiro MG. Focused ultrasound excites cortical neurons via mechanosensitive calcium accumulation and ion channel amplification. *Nature Communications* 2022; 13: 493.
35. Cotero V, Graf J, Miwa H, Hirschstein Z, Qanud K, Huerta TS, Tai N, Ding Y, Jimenez-Cowell K, Tomaio JN, Song W, Devarajan A, Tsaava T, Madhavan R, Wallace K, Loghin E, Morton C, Fan Y, Kao T-J, Akhtar K, Damaraju M, Barenboim L, Maietta T, Ashe J, Tracey KJ, Coleman TR, Di Carlo D, Shin D, Zanos S, Chavan SS, Herzog RI, Puleo C. Stimulation of the hepatoportal nerve plexus with focused ultrasound restores glucose homoeostasis in diabetic mice, rats and swine. *Nature Biomedical Engineering* 2022.
36. Silverman HA, Chen A, Kravatz NL, Chavan SS, Chang EH. Involvement of Neural Transient Receptor Potential Channels in Peripheral Inflammation. *Frontiers in Immunology* 2020; 11.
37. Guo H, Offutt SJ, Hamilton Ii M, Kim Y, Gloeckner CD, Zachs DP, Alford JK, Lim HH. Ultrasound does not activate but can inhibit in vivo mammalian nerves across a wide range of parameters. *Scientific Reports* 2022; 12: 2182.
38. Katze MG, He Y, Gale M. Viruses and interferon: a fight for supremacy. *Nature Reviews Immunology* 2002; 2: 675-687.
39. Bonnet S, Provencher S, Guignabert C, Perros F, Boucherat O, Schermuly RT, Hassoun PM, Rabinovitch M, Nicolls MR, Humbert M. Translating Research into Improved Patient Care in Pulmonary Arterial Hypertension. *American Journal of Respiratory and Critical Care Medicine* 2017; 195: 583-595.
40. Austin C, Alassas K, Burger C, Safford R, Pagan R, Duello K, Kumar P, Zeiger T, Shapiro B. Echocardiographic assessment of estimated right atrial pressure and size predicts mortality in pulmonary arterial hypertension. *Chest* 2015; 147: 198-208.
41. Lewis RA, Durrington C, Condliffe R, Kiely DG. BNP/NT-proBNP in pulmonary arterial hypertension: time for point-of-care testing? *European Respiratory Review* 2020; 29: 200009.

42. Mar PL, Nwazue V, Black BK, Biaggioni I, Diedrich A, Paranjape SY, Loyd JE, Hemnes AR, Robbins IM, Robertson D, Raj SR, Austin ED. Valsalva Maneuver in Pulmonary Arterial Hypertension: Susceptibility to Syncope and Autonomic Dysfunction. *CHEST* 2016; 149: 1252-1260.
43. George PM, Oliver E, Dorfmuller P, Dubois OD, Reed DM, Kirkby NS, Mohamed NA, Perros F, Antigny F, Fadel E, Schreiber BE, Holmes AM, Southwood M, Hagan G, Wort SJ, Bartlett N, Morrell NW, Coghlan JG, Humbert M, Zhao L, Mitchell JA. Evidence for the involvement of type I interferon in pulmonary arterial hypertension. *Circ Res* 2014; 114: 677-688.
44. Bauer EM, Zheng H, Lotze MT, Bauer PM. Recombinant Human Interferon Alpha 2b Prevents and Reverses Experimental Pulmonary Hypertension. *PLOS ONE* 2014; 9: e96720.
45. Shaffer F, Ginsberg JP. An Overview of Heart Rate Variability Metrics and Norms. *Frontiers in Public Health* 2017; 5.

Figure legends

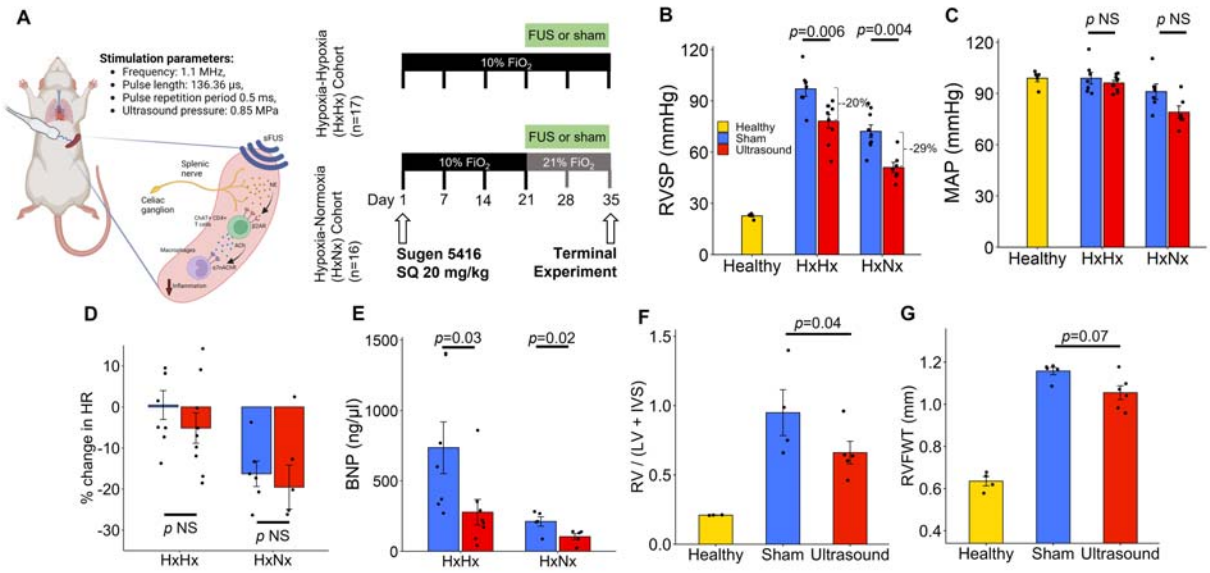

Figure 1. Focused ultrasound stimulation of the spleen improves pulmonary hemodynamics and reduces right ventricle hypertrophy in a rat model of pulmonary hypertension.

(A) Study principle, design and timeline. Focused ultrasound stimulation of the spleen (sFUS) is delivered in Sprague-Dawley rats non-invasively at 0.83 MPa, pulsing frequency of 1.1 MHz and pulse repetition period of 0.5ms, parameters that have been shown to activate an acute anti-inflammatory response in rats (21). Animals were injected subcutaneously with Sugen 5416 (20 mg/kg) and were placed in a hypoxia chamber (10% FiO_2) for 21 days (hypoxia-normoxia cohort, HxNx) or 35 days (hypoxia-hypoxia cohort, HxHx). Focused ultrasound or sham stimulation was delivered daily for 12 minutes under isoflurane anesthesia, starting at day 21 (or day 35), for 14 days. Right heart catheterization was performed at the end of treatment period. (B) Average (±SE) right ventricular systolic pressure (RVSP) in healthy animals of matched age (n=5 animals; yellow bar), in HxHx sham-treated animals (n=7; blue bar), in HxHx sFUS-treated animals (n=9; red bar), and in HxNx animals (sham, n=9; sFUS, n=7); RVSP is significantly reduced in sFUS-treated compared to sham-treated animals in both cohorts (p=0.006 and p=0.004, respectively, one-way ANOVA with Bonferroni correction). (C) Average (±SE) mean arterial pressure (MAP) in healthy animals, and in sham- and sFUS-treated animals, in the HxHx cohort (n=7 and n=9, respectively) and in the HxNx cohort (n=6 and n=6, respectively); MAP is no different between sFUS- and sham-treated animals, in either cohort (p NS, one-way ANOVA with Bonferroni correction). (D) Mean (±SE) percentage change in heart rate (HR) between first day and last day of treatment, in the HxHx and HxNx cohorts (HxHx: -5.14 ± 3.71% vs. 0.46 ± 3.51; p =0.293, HxNx: -19.53 ± 5.36 vs. -16.79% ± 3.1, p=0.61, t-test). (E) Left panel: Mean (±SE) Brain natriuretic peptide (BNP) in HxHx cohort (Sham=7; Ultrasound=9; p=0.03, one-way ANOVA). Right Panel: Mean (±SE) BNP in HxNx cohort (Sham=5; Ultrasound=6; p=0.01, t-test). BNP levels were measured in serum collected

during the terminal experiments. (F) Mean (±SE) Fulton index, calculated as RV/(LV+IVS), in healthy (n=3), sham-treated (n=4), and sFUS-treated animals (n=5) (p=0.04, one-way ANOVA with Bonferroni correction). (G) Mean (±SE) Right ventricle free wall thickness (RVFWT) obtained via the parasternal short-axis axis at the mitral valve level in healthy (n=4), sham-treated (n=5), and sFUS-treated (n=6) groups (p=0.07, one-way ANOVA with Bonferroni correction).

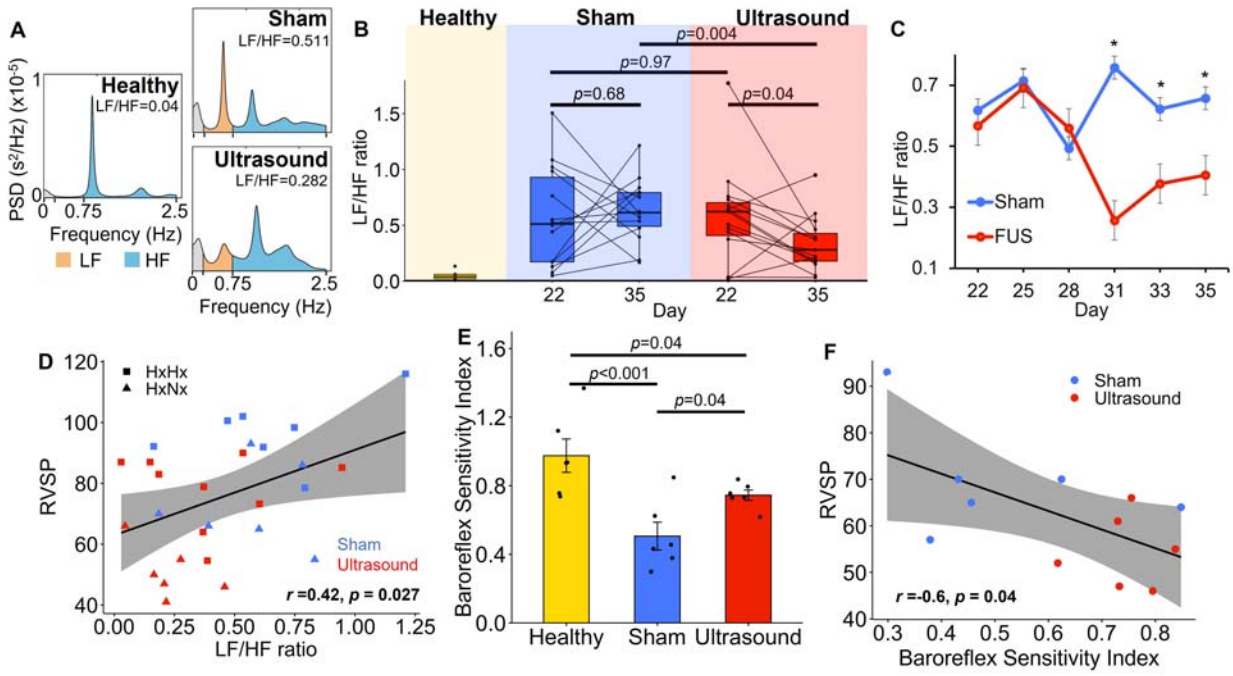

Figure 2. sFUS improves indices of autonomic function in rats with PH.

(A) Examples of heart rate power spectra used in the frequency domain analysis of heart rate variability (HRV) (62) in a healthy, sham-treated and sFUS-treated animal. The low-frequency (LF) component (0.2 to 0.75 Hz, shaded in orange) is considered an index of sympathetic activity, whereas the high-frequency (HF) component (0.75 to 2.5 Hz, shaded in blue) of parasympathetic activity. The LF/HF ratio is a metric of HRV and small LF/HF ratio is associated with a "healthier" sympathetic-parasympathetic balance. (B) LF/HF ratio on the first (day 22) and last day (day 35) of sFUS (n=15 animals) or sham treatment (n=14). LF/HF ratio is similar in the sFUS and sham groups on day 22 (p=0.97, unpaired t-test) and is reduced in sFUS on day 35 (p=0.004, unpaired t-test). When looking into the two group separately, LF/HF ratio does not change between day 22 and day 35 in the sham group (p=0.68, paired t-test), while it decreases in the sFUS group (p=0.04, paired t-test). (C) Time course of LF/HF ratio (mean±SE) throughout the treatment period, in sFUS- and sham-treated animals. Asterisks at different time points represent significant difference in LF/HF ratio between the 2 groups (p<0.05, repeated measures ANOVA). (D) Linear correlation and 95% confidence intervals (shaded area) between

RVSP and LF/HF ratio in sFUS- (blue symbols) and sham-treated animals (red symbols), in the hypoxia-normoxia (HxNx, triangles) and hypoxia-hypoxia cohorts (HxHx, squares). Pearson correlation coefficient r=-0.42 (p=0.027). (E) Mean (±SE) baroreflex sensitivity index in healthy in healthy (n=3 animals), sham-treated (n=10), and sFUS-treated animals (n=12) (ANOVA test with Bonferroni correction). BRS index was calculated as the absolute value of change in HR (|ΔHR|) over the change in systolic blood pressure (ΔSBP), before and after phenylephrine injection (25 ug/kg). (F) Linear correlation and 95% confidence intervals (shaded area) between RVSP and Baroreflex Sensitivity Index in the same animals as in panel (C) (Pearson correlation coefficient r=-0.6, p=0.04).

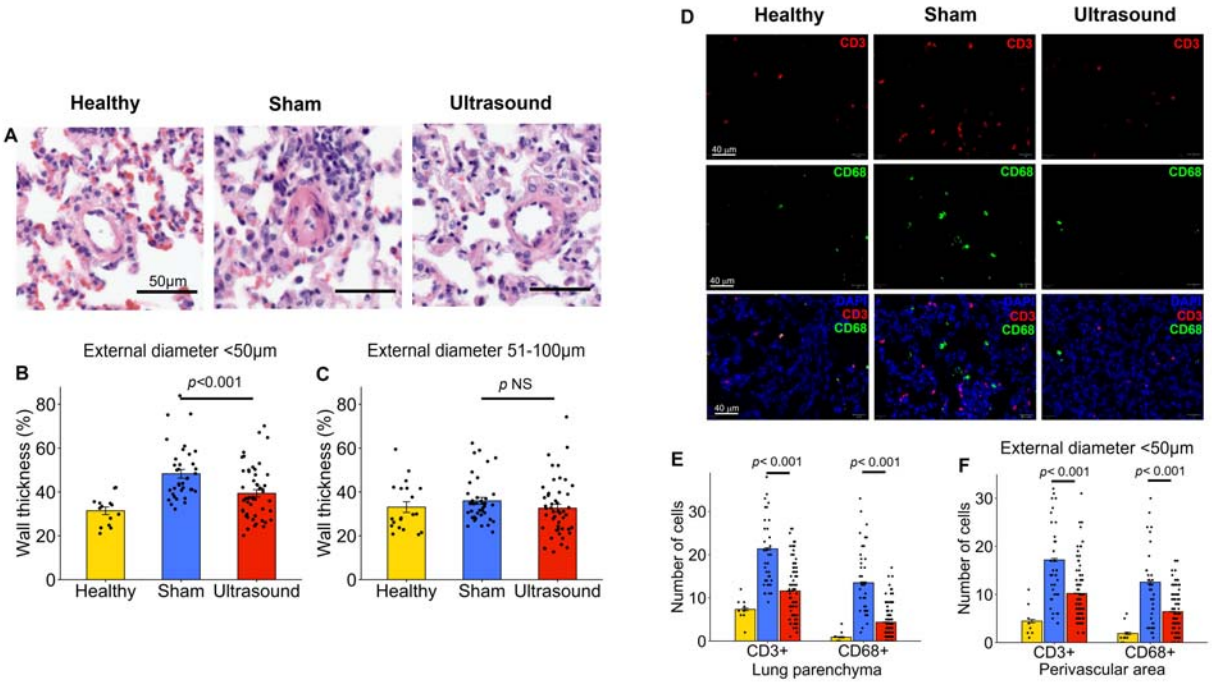

Figure 3. sFUS treatment improves vascular pathology and reduces inflammatory cell infiltration in the lung.

(A) Examples of pulmonary arterioles (PAs) in healthy, sham-treated and sFUS-treated animals, shown in Hematoxylin and eosin (H&E) stain. (B) Mean (±SE) PA wall thickness in small PAs (<50 um in external diameter) in healthy (n=2 animals), sham-treated (n=4) and sFUS-treated animals (n=5) (p=0.01, 2-way ANOVA with treatment group and animal ID as independent variables). PA wall thickness was calculated by subtracting the internal diameter of the PA from its external diameter, divided by the external diameter. Each dot represents one PA; 10 PAs per animal. (C) Same as (B), but for PAs 50-100 um in diameter (p NS). (D) Immunostaining of immune cells T-cells and macrophages in lungs of healthy, sham-treated and sFUS-treated animals. Images of lung sections stained with CD3+ antibodies (T-cells, upper panel), CD68+ antibodies (macrophages, middle panel), and both antibodies combined with nuclear DAPI stain (lower panel) in a healthy animal (left column), sham-treated animal (middle column), and sFUS-treated animal (right column). (E) Counts of CD3+ cells and CD68+ cells in healthy (1 animal),

sham-treated (2 animals), and sFUS-treated animals (4 animals) (p values from 2-way ANOVA tests). Each dot represents cell counts within a randomly selected area (150μm x 100μm) from a lung section; 10 areas per section, 2 sections per animal (1 section in the healthy animal). (F) Same as (E), but cells were counted in areas around <50 μm diameter PAs (perivascular area).

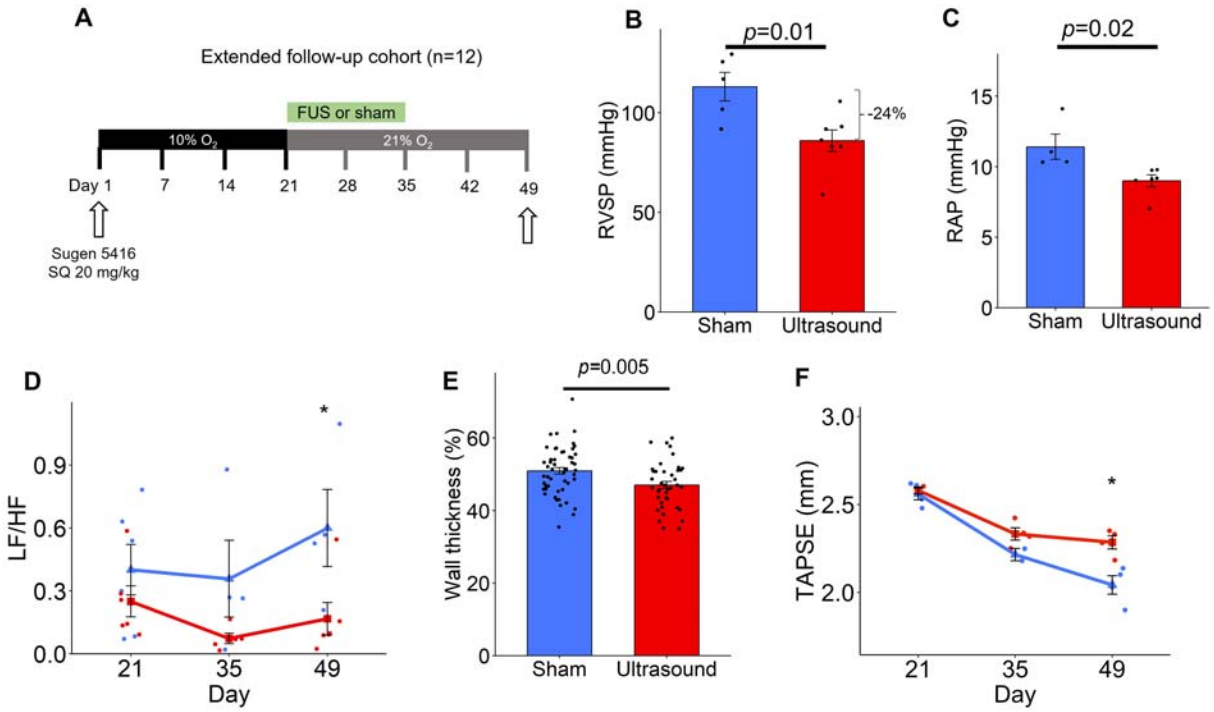

Figure 4. Therapeutic benefits of sFUS are sustained after discontinuation of treatment.

(A) Experimental timeline in an "extended follow-up" cohort: PH was induced and animals were treated with sFUS (or sham) for 2 weeks, similar to other cohorts; however, animals underwent terminal experiment 14 days after the end of treatment (day 49). (B) Mean (±SE) RVSP at day 49, 2 weeks after end of sham (N=5 animals) or sFUS treatment (N = 7) (p<0.01, t-test). (C) Mean (±SE) right atrial pressure at day 49 (sham N=4 animals vs. sFUS N = 5; p=0.02, t-test). (D) Mean (±SE) LF/HF on days 21, 35 and 49 (sham N=4, vs. sFUS N= 4). Asterisks at different time points represent significant difference between the 2 groups (*p*<0.05, repeated measures ANOVA). (E) Mean (±SE) wall thickness of small pulmonary arterioles (<50 um in diameter) (sham N=4 vs. sFUS N=5; p=0.005, 2-way ANOVA). (F) Mean (±SE) TAPSE on days 21, 35 and 49 (sham N=4, sFUS N=4). Asterisks at different time points represent significant difference between the 2 groups (*p*<0.05, repeated measures ANOVA).

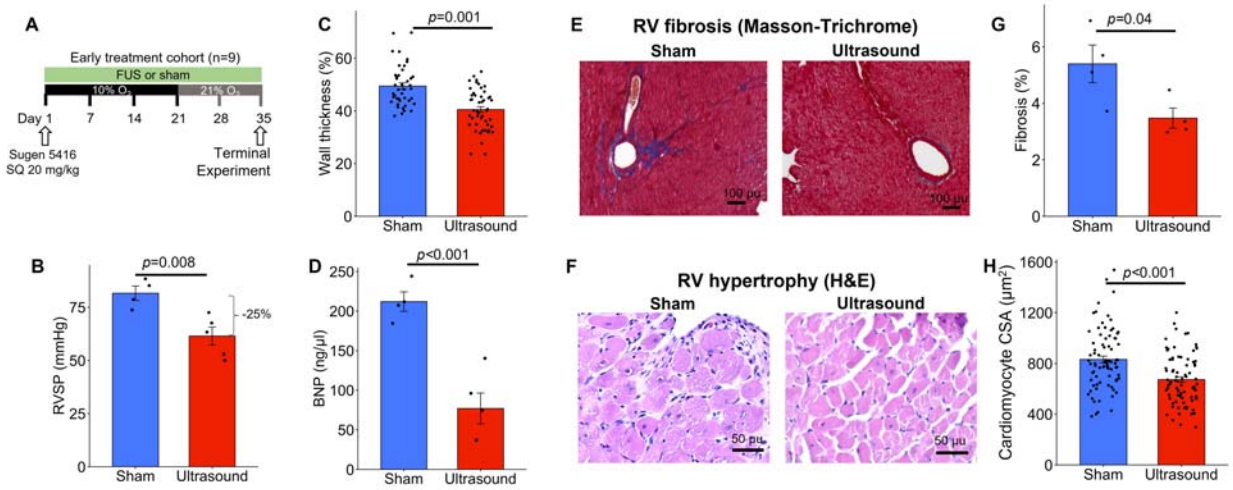

Figure 5. Therapeutic benefits of sFUS are more robust with earlier, longer treatment.

(A) Experimental timeline in an "early treatment" cohort: sFUS was initiated on the day SU5416 was injected; treatment was administered throughout the hypoxia and the normoxia period, for a total of 35 days, after which a terminal experiment occurred. (B) Mean (±SE) RVSP after 5 weeks of sFUS or sham treatment (sham N=4 animals vs. sFUS N=5 animals; p=0.008, t-test). (C) Mean (±SE) pulmonary vessel wall thickness percentage in small (<50 µm in diameter) pulmonary arterioles (p=0.001, t-test). (D) Mean (±SE) BNP levels (p<0.01, t-test). (E and F) Representative images of Masson trichrome- and hematoxylin and eosin (H&E)-stained RV sections from a sham- and ultrasound-treated animals. (G) Mean (±SE) percentage area of fibrosis in RV (p=0.04, t-test). (H) Mean (±SE) cross-sectional area (CSA) of RV cardiomyocytes (p<0.001, 2-way ANOVA). CSA values were measured in 20 randomly chosen cardiomyocytes in each animal; each dot represents one cardiomyocyte.

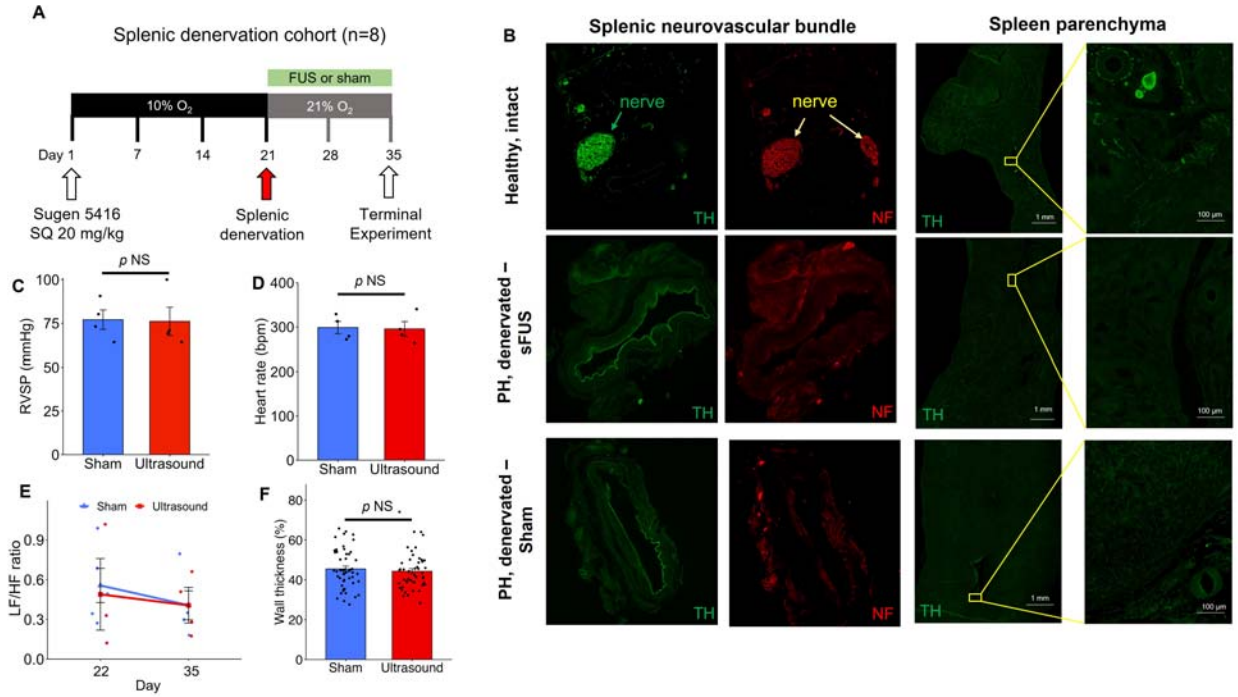

Figure 6. Selective ablation of the efferent splenic nerve eliminates the therapeutic benefit of sFUS.

(A) Experimental timeline in a "splenic denervation" cohort; at the end of hypoxia, animals undergo a survival splenic denervation procedure, followed by 14-days of sFUS (or sham) treatment and a terminal experiment. (B) Representative IHC images of adrenergic, tyrosine-hydroxylase (TH)-positive, neuronal fibers (stained together with neurofilament, NF, which stains all neuronal fibers) in the splenic neurovascular bundle (2 left-most columns) and in the spleen parenchyma (2 right-most columns) in a healthy animal with intact splenic innervation (top row), a hypertensive animal with denervated spleen that received sFUS treatment (middle row) and a hypertensive animal with denervated spleen that received sham treatment (bottom row). (C) Mean (±SE) RVSP of sham- and sFUS-treated denervated animals (Sham N=4 animals; sFUS N=4 animals; p nonsignificant, t-test). (D) Mean (±SE) heart rate (p nonsignificant, t-test). (E) Mean (±SE) LF/HF ratio (p nonsignificant, repeated measures ANOVA). (F) Mean (±SE) wall thickness (p nonsignificant, t-test).

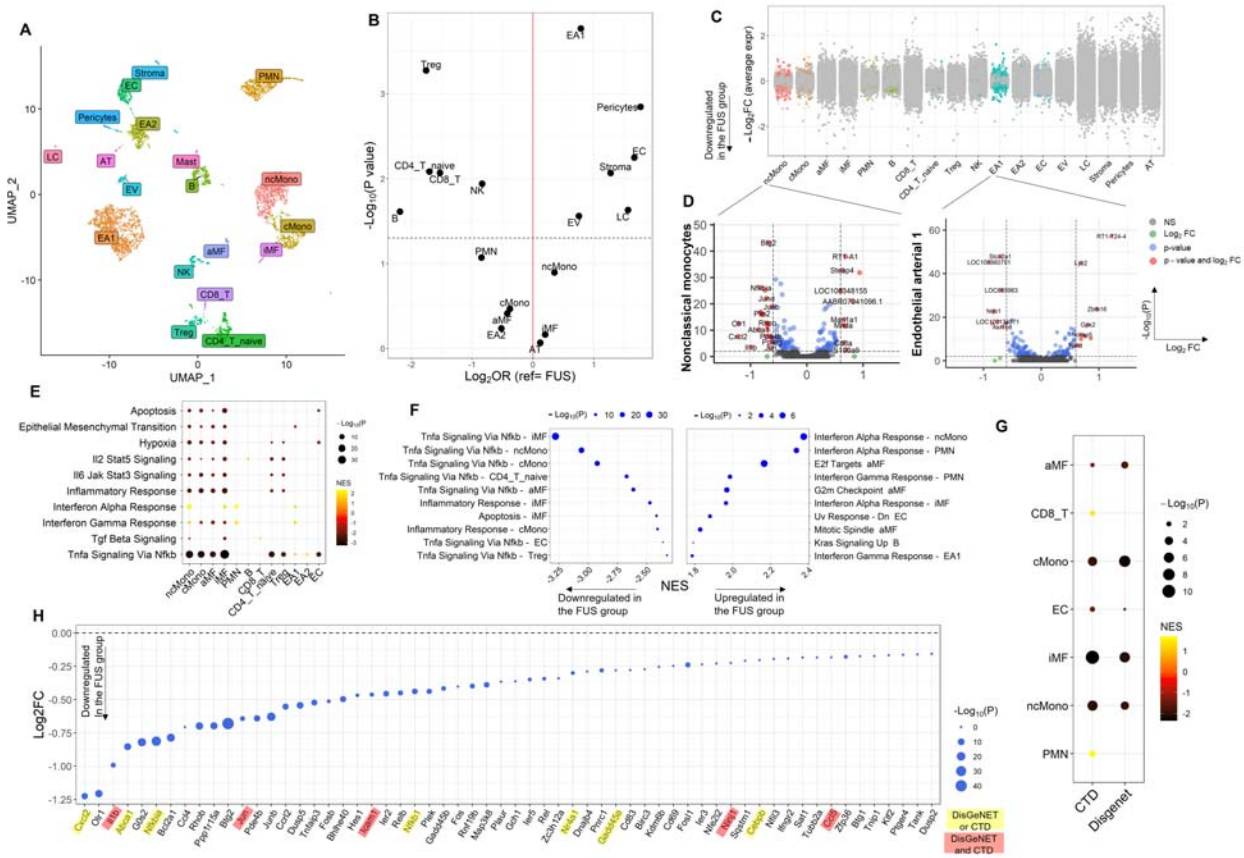

Figure 7. ScRNA-seq of the lungs from rats with PH that received FUS or sham stimulation (n=2/group). (A) Uniform manifold approximation and projection (UMAP) plot showing lung cells from 4 rats with clusters labeled by cell type. **(B)** Plot showing comparisons of the clusters size between FUS and sham-stimulated animals. X-axis represents the log2odds ratios (OR) of each cell type between FUS and sham-stimulated animals while the y-axis the –log10(P-value). The dashed line represents a p-value of 0.05. **(C)** Jitter plot showing changes in gene expression for each cell type between FUS and sham-stimulated rats. Each dot represents the differential expression MAST (Model-based Analysis of Single-Cell Transcriptomics) Log2-fold change of a gene. Dots indicating an adjusted p-value<0.05 are in color. The gray dots indicate values that were not significant (ns). **(D)** Volcano plots showing differentially expressed genes (DEGs) within the nonclassical monocytes (left) and endothelial arterial 1 (right) cells in the FUS versus sham-stimulation groups in which the x-axis represents MAST (Model-based Analysis of Single-Cell Transcriptomics) log2 fold change and the y-axis indicates -log10(P-value). **(E)** Heatmap showing major cell type-specific pathway enrichment between FUS and sham-stimulated rats using gene-set enrichment analysis (GSEA) (P<0.05) and 10 hallmark pathways from the Molecular Signatures Database that are known to be implicated in PAH on the y-axis. The dot size corresponds to -log10(P), and color represents the normalized enrichment score (NES) from GSEA, indicating upregulation (yellow) or downregulation (black). TNFa/NF-kB signaling was significantly downregulated across many cell types while interferon alpha response was the most upregulated pathway. **(F)** Dot plot showing the 10 most cell-

specific downregulated (left) and upregulated pathways (right). **(G)** Heatmap showing most highly significant ($p<0.05$) enrichment of PAH genes of Disgenet and CTD databases in cell type–specific signatures using gene-set enrichment analysis, in which yellow indicates upregulation and black/dark brown indicates downregulation. The dot size represents -Log10(p-value). Significant upregulation of PAH genes from both databases was noted in myeloid cell types. **(H)** Dot plot showing MAST (Model-based Analysis of Single-Cell Transcriptomics) log_2fold-change(Log2FC) of leading-edge genes accounting for the nonclassical monocytes downregulation of TNFa signaling via NfKb as determined by GSEA, in which the size and color tint of dots represent the -log_{10}(P-value). Highlighted gene labels represent human pulmonary arterial hypertension–associated genes from either (yellow) or both (red) of the Comparative Toxicogenomics Database and DisGeNET Databases.

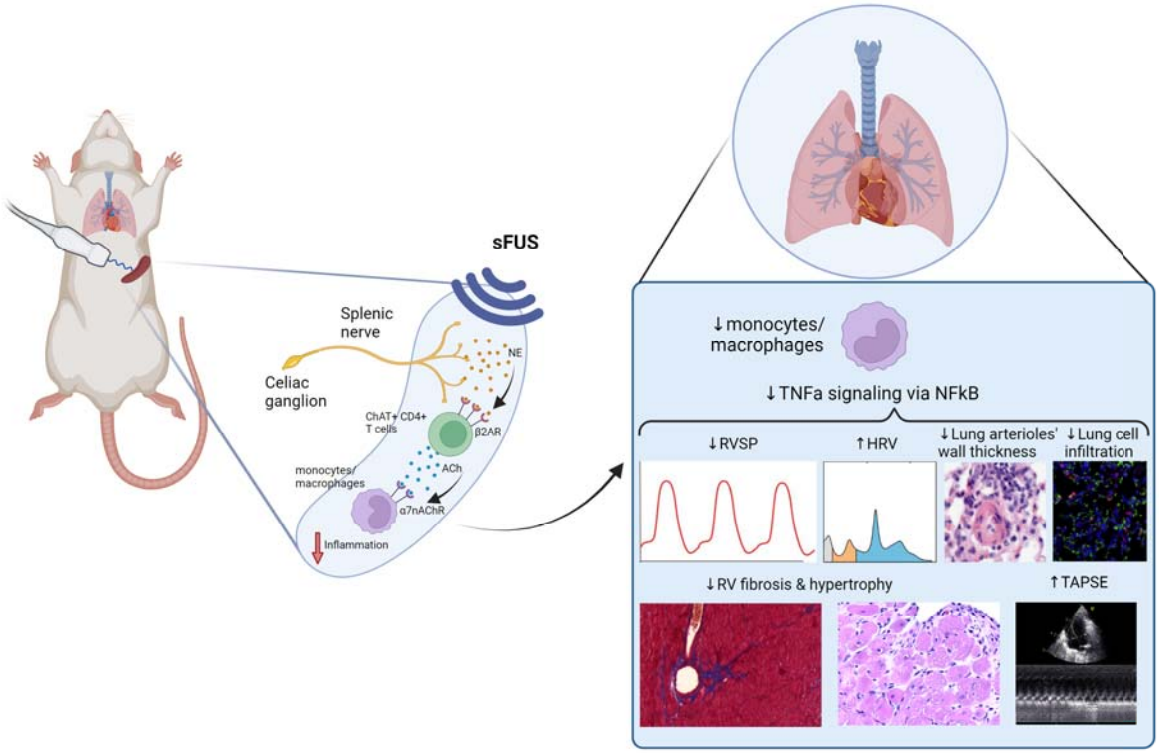

Central Illustration. In a rat model of pulmonary hypertension, sFUS for 14 days reduces monocytes/macrophages infiltration in the lungs, downregulates the TNFα signaling via NFkB pathway and results in improved pulmonary hemodynamics, autonomic indices and RV function while reduced pulmonary arterioles wall thickness and cell infiltration in the lungs, RV hypertrophy and fibrosis. RVSP, right ventricular systolic pressure; RV, right ventricle; HRV, heart rate variability; sFUS, splenic focused ultrasound stimulation; TAPSE, tricuspid annular plane systolic excursion. Created with Biorender.com